HOKKAIDO UNIVERSITY

Title	Immunolocalization of enzymes/membrane transporters related to bone mineralization in parathyroid hormone (PTH)-administered mice
Author(s)	前, 壮功仁
Degree Grantor	北海道大学
Degree Name	博士(歯学)
Dissertation Number	甲第13866号
Issue Date	2020-03-25
DOI	https://doi.org/10.14943/doctoral.k13866
Doc URL	https://hdl.handle.net/2115/94360
Type	doctoral thesis
File Information	Takahito_Mae.pdf

Hokkaido University Collection of Scholarly and Academic Papers : HUSCAP

博 士 論 文

Immunolocalization of enzymes/membrane transporters related to bone mineralization in parathyroid hormone (PTH)-administered mice

(副甲状腺ホルモン投与マウスにおける骨基質石灰化関連酵素群・膜輸送体の免疫局在)

令和 2 年 3 月申請

北海道大学

大学院歯学研究科口腔医学専攻

前　壮功仁

Immunolocalization of enzymes/membrane transporters related to bone mineralization in parathyroid hormone-administered mice

Takahito Mae

Gerontology, Graduate School of Dental Medicine, Hokkaido University, Sapporo, Japan

Abbreviated Title: *Enzymes/membrane transporters for bone mineralization*

#Address for correspondence:

Takahito Mae
Gerontology
Graduate School of Dental Medicine, Hokkaido University
Kita 13 Nishi 7 Kita-ku
Sapporo 060-8586, Japan
Tel/Fax: +81-11-706-4582
E-mail: m-a-e@den.hokudai.ac.jp

Abstract

The present study aimed to demonstrate the immunolocalization and/or gene expressions of the enzymes and membrane transporters involved in mineralization of bone after intermittent administration of parathyroid hormone (PTH). The study especially focused on TNALP, ENPP1, and PHOSPHO1, which are involved in matrix vesicle-mediated mineralization, as well as PHEX and the SIBLING family, which regulate mineralization deep inside bone. Six-week-old male mice were subcutaneously injected with 20 μg/kg/day of human PTH [1-34] two times per day (n = 6) or four times per day (n = 6) for 2 weeks. Additionally, control mice (n = 6) received vehicle. Consistent with an increase in the volume of the femoral trabeculae, the mineral appositional rate increased after PTH administration. The areas positive for PHOSPHO1, TNALP, and ENPP1 in the femoral metaphyses expanded, and the gene expressions assessed by real-time PCR were elevated in PTH-administered specimens when compared with the findings in control specimens. The immunoreactivity and/or gene expressions of PHEX and the SIBLING family (MEPE, osteopontin, and DMP1) significantly increased after PTH administration. For example, MEPE immunoreactivity was evident in some osteocytes in PTH-administered specimens, but was hardly observed in control specimens. In contrast, mRNA encoding cathepsin B was significantly reduced. Therefore, the bone matrix deep inside might be further mineralized by PHEX/SIBLING family after PTH administration. In summary, it is likely that PTH accelerate mineralization to maintain a balance with elevated matrix synthesis, presumably by mediating TNALP/ENPP1 cooperation and stimulating PHEX/SIBLING family expression.

239 words

Key words: *Mineralization, parathyroid hormone, ENPP1, TNALP, PHEX, MEPE*

Introduction

Primary bone mineralization is biologically regulated by osteoblasts that secrete matrix vesicles, small extracellular vesicles, which initiate mineralization in bone, *i.e.*, matrix vesicle-mediated mineralization [1–5]. Mature osteoblasts and matrix vesicles have several membrane transporters and enzymes, which are involved in the local supplementation of inorganic monophosphate ions (Pi), and they provide a nurturing microenvironment in the osteoid for Pi supplementation/transport, calcium phosphate nucleation and subsequent crystal growth in bone. One of the most important enzymes that can initiate mineralization in bone is tissue nonspecific alkaline phosphatase (TNALP), which can hydrolyze various phosphate esters, especially pyrophosphate (PPi), and therefore, it is responsible for the local production of Pi in bone [6–10]. Another putative inducer of mineralization is phosphoethanolamine/phosphocholine phosphatase (PHOSPHO1) [11–14], which is thought to function inside cells and matrix vesicles, catalyzing the division of phosphocholine, a constituent of the plasma membrane, into choline and Pi. In contrast to these mineralization-inducing enzymes, ectonucleotide pyrophosphatase/phosphodiesterase 1 (ENPP1) is thought to inhibit mineralization [15–18]. Crystalline structure analysis has demonstrated that extracellular adenosine triphosphate (ATP) is accommodated in a pocket formed by an insertion loop of ENPP1, explaining the preference of ENPP1 for an ATP substrate [19]. Additionally, ankylosis (ANK), a non-enzymatic plasma-membrane PPi channel, might allow intracellular PPi to pass through the cell membrane from the cytoplasm to the outside of the cell [20, 21]. The resultant extracellular PPi can serve as an inhibitor of mineralization to avoid pathological mineralization [21]. However, in bone, extracellular PPi is hydrolyzed by TNALP to Pi, which is used for the constituents of mineral crystals. Therefore, finally-tuned cooperation/activities of these enzymes and membrane transporters in the osteoid, which is the site of primary mineralization in bone, appears to be necessary for normal mineralization in bone.

Fibroblast growth factor 23 (FGF23) is expressed in bone, especially in osteocytes, and it circulates to the renal proximal tubules to bind the FGFR1c/αklotho receptor complex in order to reduce the reabsorption of Pi in the kidneys [22–26]. However, recent studies have proposed an autocrine function of FGF23, which, at least in part, is related to bone mineralization.

Osteoblasts/osteocytes express not only FGF23 but also the FGFR1c/αklotho receptor complex [27, 28], consequently regulating bone mineralization in an autocrine manner [29]. In addition, PHEX, which is responsible for X-linked hypophosphatemic rickets [30], has been postulated to inhibit FGF23 expression for the control of the serum Pi concentration, as well as to bind the small integrin-binding ligand N-linked glycoprotein (SIBLING) family for the local regulation of mineralization in bone [31–33]. The SIBLING family includes osteopontin, matrix extracellular phosphoglycoprotein (MEPE), dentin matrix protein 1 (DMP1), dentin sialoprotein, and bone sialoprotein [34–36], and it has been thought to be hydrolyzed by cathepsin B to generate ASARM peptides. The serine residues of ASARM peptides are then phosphorylated to form pASARM, which can bind hydroxyapatite crystals, consequently inhibiting mineral crystal growth [37, 38]. On the contrary, PHEX has been documented to bind the SIBLING family and block the hydrolysis of cathepsin B, consequently avoiding the synthesis of ASARM peptides [38, 39]. Therefore, PHEX, which regulates FGF23 expression in bone and inhibits pASARM synthesis from the SIBLING family, appears to play a pivotal role in both systemic regulation of the serum Pi concentration and local mineralization in bone, especially deep inside bone.

Parathyroid hormone (PTH) is a calcitropic hormone that systemically increases the serum concentration of calcium (Ca) by increasing bone turnover and Ca reabsorption in the kidneys, as well as stimulating 1α-hydroxylase activity in the renal proximal tubules. On the other hand, PTH reduces the serum Pi concentration by inhibiting the reabsorption of Pi in kidneys, and it has been shown to increase the synthesis of FGF23 in bone to indirectly inhibit the reabsorption of Pi in the kidneys [40]. Despite the opposing effects of PTH on serum Ca and Pi, it is well-known that intermittent administration of PTH [1-34] induces bone formation and mineralization [41, 42]. This might imply that PTH can facilitate bone mineralization accompanied with increasing bone formation by affecting enzymes and membrane transporters involved in mineralization, rather than affecting the serum concentrations of Ca and Pi.

Thus, TNALP, ENPP1, and PHOSPHO1 appear to be involved in primary mineralization in the osteoid, *i.e.,* matrix vesicle-mediated mineralization, whereas PHEX, FGF23, the SIBLING family (MEPE, osteopontin, etc.), and cathepsin B might be associated with the regulation of mineralization deep inside bone that has been mineralized. In addition, PTH

appears to accelerate mineralization in bone, presumably affecting the enzymes and membrane transporters related to bone mineralization, rather than mediating the serum concentrations of Ca and Pi. Therefore, the present study aimed to demonstrate the immunolocalization and/or gene expressions of the enzymes and membrane transporters involved in the mineralization of bone (TNALP, ENPP1, PHOSPHO1, PHEX, MEPE, etc.) after intermittent administration of PTH.

Materials and Methods

Animals

Six-week-old male C57BL/6J mice (n = 18, Japan CLEA, Tokyo, Japan) were used in this study. The study followed the principles for animal care and research use set by Hokkaido University (approval no.: 15-0032). According to our previous study [42], 20 μg/kg/day of human PTH [1-34] (Sigma-Aldrich Co., LLC., St. Louis, MO) was subcutaneously injected two times per day (n = 6) or four times per day (n = 6) into the study mice for 2 weeks. Age-matched mice that underwent vehicle administration were used as controls (n = 6).

Preparation of histochemical specimens

Before fixation, mice were anesthetized with an intraperitoneal injection of chloral hydrate for body weight determination and blood collection to estimate the concentrations of serum Ca and Pi. The left hind legs of the mice were ligated at the femoral region, and the left tibiae were extracted for analyses involving reverse transcription polymerase chain reaction (RT-PCR) and real-time PCR, as described later. All mice were then perfused with 4% paraformaldehyde diluted in 0.1 M cacodylate buffer (pH 7.4) through the cardiac left ventricle. The right tibiae and femora were immediately removed and immersed in the same fixative for 18 h at 4°C. The samples were decalcified with a solution of 10% ethylene diamine tetraacetic disodium salt and were dehydrated in ascending ethanol solutions prior to paraffin embedding for immunohistochemical examination. For von Kossa staining, undecalcified tibiae were post-fixed with 1% osmium tetraoxide in a 0.1 M cacodylate buffer for 4 h at 4°C, dehydrated in ascending acetone solutions, and embedded in epoxy resin (Epon 812, Taab, Berkshire, UK) [43].

Immunostaining of TNALP, ENPP1, PHOSPHO1, FGF23, osteopontin, and MEPE

Dewaxed paraffin sections were examined for TNALP as previously reported [44, 45]. In brief, after inhibition of endogenous peroxidases with methanol containing 0.3% hydrogen peroxidase for 30 min, dewaxed paraffin sections were pretreated with 1% bovine serum albumin (BSA; Serologicals Proteins Inc. Kankakee, IL) in PBS (1% BSA-PBS) for 30 min. Sections were then incubated for 2–3 h at room temperature (RT) with rabbit polyclonal antisera against TNALP [9] at a dilution of 1:300 (1% BSA-PBS). This was followed by incubation with horseradish (HRP)-conjugated anti-rabbit IgG (Jackson Immunoresearch Laboratories Inc., West Grove, PA). For FGF23, after pre-incubation with 1% BSA-PBS for 30 min at RT, sections

were incubated with rat anti-FGF23 antibodies (R&D Systems Inc., Minneapolis, MN) at a dilution of 1:100 for 2 h [42] and then incubated with HRP-conjugated anti-rat IgG (Chemicon International Inc., Temecula, CA) at a dilution of 1:100 for 1 h. For ENPP1, sections were incubated with goat polyclonal anti-ENPP1 (Everest Biotech Ltd., Oxfordshire, UK) at a dilution of 1:200 for 1 h and then incubated with HRP-conjugated rabbit anti-goat IgG (American Qualex Scientific Products, Inc., San Clemente, CA). For PHOSPHO1, sections were initially incubated with human monoclonal anti-PHOSPHO1 (Bio-Rad Laboratories Inc., Hercules, CA) at a dilution of 1:100. Subsequently, the sections were incubated with rabbit anti-myc Tag (Medical & Biological Laboratories Co., Ltd., Nagoya, Japan) and then incubated with HRP-conjugated swine anti-rabbit IgG (Agilent Technologies, Inc., Santa Clara, CA) at a dilution of 1:100. For osteopontin and MEPE, dewaxed sections were reacted with rabbit antibodies against mouse osteopontin (LSL Co., Ltd., Tokyo, Japan) at a dilution of 1:2000 or rabbit polyclonal antibodies against MEPE (Cloud-Clone Corp., Katy, TX) at a dilution of 1:100 (1% BSA-PBS) for 2 h. Following several washings in PBS, they were then incubated with HRP-conjugated anti-rabbit IgG (Jackson Immunoresearch Laboratories Inc.) for 1 h. To visualize all HRP-conjugated immunoreactions, diaminobenzidine tetrahydrochloride was used as a substrate. All sections were counterstained with methyl green and observed under a light microscope (Eclipse Ni, Nikon Instruments Inc., Tokyo, Japan).

Immunofluorescent staining for the detection of TNALP and ENPP1

For the detection of TNALP and ENPP1, dewaxed paraffin sections were incubated with 1% BSA-PBS and then with rabbit polyclonal antibodies against TNALP at a dilution of 1:300 (1% BSA-PBS). Subsequently, they were incubated with Alexa Fluor 594-conjugated goat anti-rabbit IgG (Thermo Fisher Scientific, Inc., Waltham, MA) at a dilution of 1:100 (1% BSA-PBS) for 1 h and then with goat polyclonal anti-ENPP1 at a dilution of 1:200 (1% BSA-PBS) after washing with PBS. Additionally, the sections were incubated with Alexa Fluor 488-conjugated donkey anti-goat IgG (Thermo Fisher Scientific, Inc.) at a dilution of 1:100 (1% BSA-PBS) for 1 h. After embedding the sections using VECTASHIELD hard-set mounting medium with DAPI (Vector Laboratories, Inc. Burlingame, CA), the sections were observed under a light microscope.

Von Kossa staining

Epoxy resin sections from undecalcified specimens were incubated with an aqueous solution of silver nitrate until dark brown/black staining of bone tissue was discernible under a light

microscope [46].

Measurement of serum Ca and Pi

Serum samples were stored at −30°C before the assays. The serum concentrations of Ca and Pi were quantified by Oriental Yeast Co., Ltd., using enzymatic methods.

Mineral appositional rate after PTH administration

A 600 × 600 μm region of interest located 150 μm below the growth plate of the tibial metaphysis was used for the assessment of the static parameters of inter-labels width (It.L.Th) and inter-label time (It.L.t., 4 days). Then, the mineral appositional rate (MAR) was calculated. Abbreviations and calculations were used according to the recommendations of the ASBMR Histomorphometry Nomenclature Committee, whenever possible [47].

PCR and real-time PCR

Left tibiae harvested from control mice and PTH-administered mice, as described above, were immediately frozen in liquid nitrogen and crushed into small pieces. The crushed specimens were homogenized in 10 mL of TRIzol reagent (Life Technologies Co., Carlsbad, CA) per 1 g tissue to extract total RNA. The mixture was centrifuged at 15,000 rpm for 5 min at 4°C, allowing for the removal of small debris. The supernatant was transferred to a new tube, which was vortexed for 15 s after adding 2 mL of chloroform. The lysate was then transferred to a new tube and was incubated for 5 min at RT. After phase separation, the aqueous phase containing RNA was transferred to a new tube, and RNA was precipitated by adding 5 mL of isopropyl alcohol per 10 mL of TRIzol reagent. After incubation for 10 min at RT, the mixture was centrifuged at 15,000 rpm for 60 min at 4°C. The resulting RNA pellet was washed with 1 mL of 75% ethanol and was briefly air-dried. The RNA pellet was dissolved in 30 μL of diethyl pyrocarbonate-treated water. First-strand cDNA was synthesized from 2 μg of total RNA by using the SuperScript VILO cDNA Synthesis Kit (Life Technologies).

The primer sequences used for PCR were as follows: mouse Gapdh forward: TGTCTTCACCACCATG GAGAAGG, reverse: GTGGATGCAGGGATGATGTT CTG; mouse Tnalp forward: GCCCTCTCCAAGACATATA, reverse: CCATGATCACGTCGATATCC; mouse Enpp1 forward: TATTGGCTATGGACCTGCCTTCAAGC, reverse: GTAGAATCCGGGGCCTCCCGTAG; mouse Phospho1 forward: GACAATGAGCGGGTGTTTTC, reverse: GGGGATGGTCTCGTAGACAG; mouse Ank forward: GAAATCCGGGCTGTCTACCC,

reverse: TCAGTGTCATCAGCCATCCAG; mouse FgfF23 forward: TGTCAGATTTCAAACTCAG, reverse: GGATAGGCTCTAGCAGTG; mouse Fgfr1c forward: CTTGACGTCGTGGAAC GATCT, reverse: AGAACGGTCAACCATGCAGAG; mouse αKlotho forward: GGGTCACTGGGTCA ATCT, reverse: GCAAAGTAGCCACAAAGG; mouse Mepe forward: CCCCAAGAGCAGCAAAGGTA, reverse: CTCCGCTGTGACATCCCTTTA; and mouse Phex forward: TTCTGATGGAAGCAGAAACAGGGA, reverse: GGGAATCATAGCGCTGAGTTCTGA. PCR was performed using a thermal cycler (GeneAmp PCR System 2700; Applied Biosystems, Foster City, CA) as follows: denaturation at 94°C for 30 s; annealing at 60°C (for Gapdh, Ank, Phospho1, Phex, and Mepe), 53°C (for Fgf23), 55°C (for Fgfr1c and αKlotho), 56°C (for Tnalp), or 63°C (for Enpp1) for 30 s; extension at 72°C for 30 s; and final incubation at 72°C for 10 min. RT-PCR products were subjected to 2% agarose gel electrophoresis, stained with ethidium bromide, and detected using E-Gel Imager (Life Technologies).

Real-time PCR assays were performed using Taqman probes (Applied Biosystems) for the gene expressions of Alpl (Mm00475834_m1), Enpp1 (Mm01193761_m1), Phospho1 (Mm07301398_m1), Ank (Mm00445040_m1), Mepe (Mm02525159_s1), Phex (Mm00448119_m1), Fgf23 (Mm00445621_m1), Fgfr1 (Mm00438930_m1), Osteopontin (Mm00436767_m1), Dmp1 (Mm01208363_m1), and Cathepsin B (Mm01310506_m1). These gene expressions were detected using the StepOne Real-Time PCR System (Applied Biosystems), and they were normalized to Gapdh (Mm99999915_g1) expression using the 2ΔΔCt method.

Statistical analysis

All values are presented as mean ± standard error. All statistical analyses were carried out using BellCurve for Excel version 2.00 (Social Survey Research Information Co., Ltd., Tokyo, Japan) and analyzed for statistical significance by Student's t-test. A P-value <0.05 was considered significant.

Results

Metaphyseal bone mineralization and immunolocalization of PHOSPHO1, TNALP, and ENPP1

The bone volume of the femoral metaphyses was higher in two times and four times PTH-administered specimens than in control specimens **(Figs. 1A-C)**. Von Kossa staining showed a thick zone of incompletely mineralized osteoid in the PTH-administered trabeculae, but not in the control counterparts **(Figs. 1D-F)**. Additionally, the MAR index was significantly higher in four times PTH-administered specimens than in control specimens (2.19 ± 0.05 vs. 1.47 ± 0.12, $P < 0.01$) **(Fig. 1G)**. There was no significant difference in the serum Ca concentration, but the serum Pi concentration was significantly lower in PTH-administered specimens than the control specimens (8.56 ± 0.51 vs. 10.46 ± 0.66, $P < 0.01$) **(Fig. 1H)**.

The areas positive for PHOSPHO1 appeared to expand after PTH administration **(Figs. 2A-C)**, and PHOSPHO1 immunoreactivity was mainly localized on the surface of mature osteoblasts in both the control and PTH-administered specimens **(Figs. 2D-F)**. The immunoreactivity of TNALP, which hydrolyzes PPi to Pi, was markedly-intense in PTH-administered metaphyses when compared with the findings in control counterparts **(Figs. 3A-C)**. At higher magnification, not only osteoblasts but also preosteoblastic cells appeared to show intense TNALP immunoreactivity **(Figs. 3D-F)**. ENPP1, which provides PPi, was broadly observed in osteoblasts in the PTH-administered metaphyseal trabeculae, whereas it was slightly observed in osteoblasts in the control counterparts **(Figs. 3G-L)**.

Double immunofluorescent analysis demonstrated that in control specimens, ENPP1 was mainly localized throughout the cytoplasmic region of osteoblasts and TNALP was roughly observed on the cell membrane **(Figs. 4A-D)**. On the other hand, in PTH-administered specimens, TNALP and ENPP1 seemingly overlapped in osteoblastic cells, although some osteoblastic cells showed intense ENPP1 reactivity **(Figs. 4E-H)**.

Immunolocalization of FGF23, MEPE, and osteopontin in the bone matrix

We examined the immunolocalization of FGF23, MEPE, and osteopontin, which are related to the PHEX/SIBLING family axis. FGF23 immunoreactivity was detected in osteocytes in the control femora, but was detected in both osteoblasts and osteocytes in the PTH-administered counterparts **(Figs. 5A-C)**. MEPE was hardly observed in the control femora, but was evident in some osteocytes in the PTH-administered counterparts **(Figs. 5D-F)**. There appeared to be many osteopontin-immunopositive lines identical to cement lines after PTH administration

(Figs. 5G-I). There was no apparent difference in the immunolocalization of FGF23, osteopontin, or MEPE between the regimens of two times and four times per day of PTH-administration.

Gene expressions of Tnalp, Enpp1, Phospho1, Ank, Mepe, Phex, Fgf23, Fgfr1, αKlotho, Osteopontin, Dmp1, and Cathepsin B

We examined the gene expressions of Tnalp (Alpl), Enpp1, Phospho1, Ank, Mepe, Phex, Fgf23, Fgfr1, αKlotho, Osteopontin, Dmp1, and Cathepsin B using RT-PCR and/or real time PCR. All genes tended to be elevated on assessment with RT-PCR **(Figs. 6A, 7A)**. Therefore, we quantified the expressions of the genes in control specimens and PTH-administered specimens by using real-time PCR **(Figs. 6C-H)**. The indices of Tnalp (Alpl), Enpp1, Phospho1, Ank, Mepe, Phex, Fgf23, Fgfr1, Osteopontin, and Dmp1 were 2.7 ($P < 0.01$), 1.8 ($P < 0.05$), 2.8 ($P < 0.01$), 1.3 ($P < 0.01$), 2.0 ($P < 0.01$), 4.4 ($P < 0.01$), 1.4 ($P < 0.01$), 2.2 ($P < 0.01$), 2.5 ($P < 0.01$), and 2.6 ($P < 0.01$) times higher in four times PTH-administered specimens when compared with the findings in control specimens **(Figs. 6B-E, Figs. 7B-G).** However, the index of Cathepsin B was 0.9 times ($P < 0.05$) lower in four times PTH-administered specimens when compared with the findings in control specimens **(Fig. 7H)**.

Discussion

The present study attempted to histochemically elucidate the immunolocalization and gene expressions of enzymes and membrane transporters involved in matrix vesicle-mediated mineralization, as well as the regulation of mineralization by PHEX/SIBLING family after PTH administration. Immunohistochemistry and real-time PCR indicated increased expressions of TNALP, ENPP1, and PHOSPHO1, which are involved in matrix vesicle-mediated mineralization in the osteoid, consistent with an elevated MAR index. Phex gene expression was markedly-increased (4.4 times) in PTH-administered specimens when compared with the findings in control specimens. On the other hand, Cathepsin B gene expression decreased, although mRNAs encoding MEPE, osteopontin, and DMP1 of the SIBLING family increased. These findings might lead to the assumption that bone matrix, which has been previously subjected to matrix vesicle-mediated mineralization, might be further mineralized to maintain a balance with the promoted synthesis of matrix proteins through PHEX/SIBLING family after PTH administration. Thus, it seems likely that PTH would accelerate mineralization to maintain a balance with elevated matrix synthesis, presumably by mediating TNALP/ENPP1 cooperation and stimulating PHEX/SIBLING family expression.

TNALP expression and the areas of TNALP-immunoreactive osteoblasts/preosteoblasts markedly-increased, and consistently, PHOSPHO1 expression was more evident in the PTH-administered trabeculae. However, the distribution patterns of TNALP and PHOSPHO1 did not change after PTH administration. TNALP was maintained in both preosteoblastic cells and mature osteoblasts, whereas PHOSPHO1 was localized on the surface of mature osteoblasts even after PTH administration. On the other hand, some osteoblastic cells showed relatively-intense ENPP1-positivity, presumably implying that these ENPP1-intense osteoblastic cells can regulate mineralization by synthesizing abundant PPi to inhibit excess mineralization. This appears reasonable when considering reports that extracellular PPi derived from ENPP1 activities inhibited mineralization by preventing overgrowth of crystals [15–18]. Therefore, it appears likely that PTH might elevate the expressions of TNALP and PHOSPHO1 to facilitate mineralization and might simultaneously promote ENPP1 expression to regulate excessive mineralization. However, further examinations are necessary to identify which cell-types show intense ENPP1 immunoreactivity.

Consistent with the findings in a previous report [40], the intermittent administration of PTH in this study resulted in increased expression of FGF23. Our previous study demonstrated that intermittent administration of PTH did not induce significant changes in the serum

concentrations of Ca and Pi [42]. However, the present study demonstrated a significant decrease in the serum Pi concentration after PTH administration. The reduced serum Pi might be associated with direct PTH action on the kidneys and indirect action mediating the FGF23/αklotho axis that cooperates with the kidneys [48].

Interestingly, not only osteocytes but also osteoblasts showed intense FGF23 immunoreactivity after PTH administration **(Fig. 5A-C)**. Our previous report localized FGF23 in osteoblasts and osteocytes in the embryonic and neonatal bones, indicating that FGF23 signaling might be involved in bone formation rather than in the systemic regulation of serum Pi at these developmental stages [28]. Recent reports have mentioned that osteoblast/osteocyte-derived FGF23 inhibited PHEX expression by mediating FGFR1c/αklotho in an autocrine manner [29], and also that FGF23 synthesized by osteocytes can reduce TNALP expression by mediating FGFR3, which is independent of the FGF23/αklotho axis [49]. These findings indicate an alternative pathway of FGF23 signaling in bone without mediation of the αklotho/FGFR1c receptor in the kidneys.

Expression of the Phex gene markedly-increased 4.4 times and that of the Cathepsin B gene reduced 0.9 times in PTH-administered specimens when compared with the findings in control specimens. Considering that PHEX binds to the SIBLING family to block hydrolysis by cathepsin B, the increased expression of Phex and reduced expression of Cathepsin B could allow further mineralization in bone by reducing the production of phosphorylated ASARM that inhibits mineralization. As MEPE and osteopontin were localized in the regions of osteocytes and cement lines, respectively, further mineralization by PHEX/SIBLING family might occur not in the osteoid but in the deep portion of the bone matrix.

In summary, PTH seems facilitate the gene expressions and protein levels of TNALP, PHOSPHO1, and ENPP1 to induce mineralization in the osteoid while maintaining a balance with the accelerated synthesis of matrix proteins, as well as stimulating the expressions of PHEX and the SIBLING family but reducing the expression of cathepsin B, consequently inducing further mineralization in the deep portion of the bone matrix.

References

1. Hasegawa T, Yamamoto T, Tsuchiya E, Hongo H, Tsuboi K, Kudo A, Abe M, Yoshida T, Nagai T, Khadiza N, Yokoyama A, Oda K, Ozawa H, Freitas de PHL, Li M, Amizuka N (2017) Ultrastructural and biochemical aspects of matrix vesicle-mediated mineralization. Jpn Dent Sci Rev 53:34–45

2. Hasegawa T (2018) Ultrastructure and biological function of matrix vesicles in bone mineralization. Histochem Cell Biol 149:289–304

3. Ozawa H (1985) Ultrastructural concepts on biological calcification; Focused on matrix vesicles. J Oral Bioscience 27:751–774

4. Ozawa H, Hoshi K, Amizuka N (2008) Current concepts of bone mineralization. J Oral Biosci 50:1–14

5. Amizuka N, Hasegawa T, Oda K, Luiz de Freitas PH, Hoshi K, Li M, Ozawa H (2012) Histology of epiphyseal cartilage calcification and endochondral ossification. Front Biosci 4:2085–2100

6. de Bernard B, Bianco P, Bonucci E, Costantini M, Lunazzi GC, Martinuzzi P, Modricky C, Moro L, Panfili E, Pollesello P (1986) Biochemical and immunohistochemical evidence that in cartilage an alkaline phosphatase is a Ca^{2+}-binding glycoprotein. J Cell Biol 103:1615–1623

7. Matsuzawa T, Anderson HC (1971) Phosphatases of epiphyseal cartilage studied by electron microscopic cytochemical methods. J Histochem Cytochem 19:801–808

8. Nakano Y, Beertsen W, van den Bos T, Kawamoto T, Oda K, Takano Y (2004) Site-specific localization of two distinct phosphatases along the osteoblast plasma membrane: tissue non-specific alkaline phosphatase and plasma membrane calcium ATPase. Bone 35:1077–1085

9. Oda K, Amaya Y, Fukushi-Irie M, Kinameri Y, Ohsuye K, Kubota I, Fujimura S, Kobayashi J (1999) A general method for rapid purification of soluble versions of glycosylphosphatidylinositol-anchored proteins expressed in insect cells: an application for human tissue-nonspecific alkaline phosphatase. J Biochem 126:694–699

10. Hoshi K, Amizuka N, Oda K, Ikehara Y, Ozawa H (1997) Immunolocalization of tissue non-specific alkaline phosphatase in mice. Histochem Cell Biol 107:183–191

11. Houston B, Seawright E, Jefferies D, Hoogland E, Lester D, Whitehead C, Farquharson C (1999) Identification and cloning of a novel phosphatase expressed at high levels in differentiating growth plate chondrocytes. Biochim Biophys Acta 1448:500–506

12. Houston B, Stewart AJ, Farquharson C (2004) PHOSPHO1–A novel phosphatase specifically expressed at sites of mineralisation in bone and cartilage. Bone 34:629–637

13. Roberts S, Narisawa S, Harmey D, Millán JL, Farquharson C (2007) Functional involvement of PHOSPHO1 in matrix vesicle-mediated skeletal mineralization. J Bone Miner Res 22:617–627

14. Roberts SJ, Stewart AJ, Sadler PJ, Farquharson C (2004) Human PHOSPHO1 exhibits high specific phosphoethanolamine and phosphocholine phosphatase activities. Biochem J 382:59–65

15. Takahashi T, Old LJ, Boyse EA (1970) Surface alloantigens of plasma cells. J Exp Med 131:1325–1341

16. Johnson K, Moffa A, Chen Y, Pritzker K, Goding J, Terkeltaub R (1999a) Matrix vesicle plasma membrane glycoprotein-1 regulates mineralization by murine osteoblastic MC3T3 cells. J Bone Miner Res 14:883–892

17. Johnson K, Vaingankar S, Chen Y, Moffa A, Goldring M, Sano K, Jin-Hua P, Sali A, Goding J, Terkeltaub R (1999b) Differential mechanisms of inorganic pyrophosphate production by plasma cell membrane glycoprotein-1 and B10 in chondrocytes. Arthritis Rheum 42:1986–1997

18. Terkeltaub R, Rosenbach M, Fong F, Goding J (1994) Causal link between nucleotide pyrophosphohydrolase overactivity and increased intracellular inorganic pyrophosphate generation demonstrated by transfection of cultured fibroblasts and osteoblasts with plasma cell membrane glycoprotein-1. Arthritis Rheum 37:934–941

19. Kato K, Nishimasu H, Okudaira S, Mihara E, Ishitani R, Takagi J, Aoki J, Nureki O (2012) Crystal structure of Enpp1, an extracellular glycoprotein involved in bone mineralization and insulin signaling. Proc Natl Acad Sci USA 109:16876–16881

20. Gurley KA, Reimer RJ, Kingsley DM (2006) Biochemical and genetic analysis of ANK in arthritis and bone disease. Am J Hum Genet 79:1017–1029

21. Ho AM, Johnson MD, Kingsley DM (2000) Role of the mouse ank gene in control of tissue calcification and arthritis. Science 289:265–270

22. Lorenz-Depiereux B, Grabowski M, Meitinger T, Strom TM (2000) Autosomal dominant hypophosphataemic rickets is associated with mutations in FGF23. Nat Genet 26:345–348

23. Shimada T, Hasegawa H, Yamazaki Y, Muto T, Hino R, Takeuchi Y, Fujita T, Nakahara K, Fukumoto S, Yamashita T (2004) FGF-23 is a potent regulator of vitamin D metabolism and phosphate homeostasis. J Bone Miner Res 19:429–435

24. Kurosu H, Ogawa Y, Miyoshi M, Yamamoto M, Nandi A, Rosenblatt KP, Baum MG, Schiavi S, Hu MC, Moe OW, Kuro-o M (2006) Regulation of fibroblast growth factor-23 signaling by klotho. J Biol Chem 281:6120–6123

25. Urakawa I, Yamazaki Y, Shimada T, Iijima K, Hasegawa H, Okawa K, Fujita T, Fukumoto S, Yamashita T (2006) Klotho converts canonical FGF receptor into a specific receptor for FGF23. Nature 444:770–774

26. Hasegawa T, Sasaki M, Yamada T, Ookido I, Yamamoto T, Hongo H, Yamamoto T, Oda K, Yokoyama K, Amizuka N (2013) Histochemical examination of vascular medial calcification of aorta in klotho-deficient mice. J Oral Biosci 55:10–15

27. Kawai M, Kinoshita S, Shimba S, Ozono K, Michigami T (2014) Sympathetic activation induces skeletal Fgf23 expression in a circadian rhythm-dependent manner. J Biol Chem 289:1457–1466

28. Sakurai A, Hasegawa T, Kudo A, Shen Z, Nagai T, Abe M, Yoshida T, Hongo H, Yamamoto T, Yamamoto T, Oda K, Freitas de PHL, Li M, Sano H, Amizuka N (2017) Chronological immunolocalization of sclerostin and FGF23 in the mouse metaphyseal trabecular and cortical bone. Biomed Res 38:257–267

29. Minamizaki T, Konishi Y, Sakurai K, Yoshioka H, Aubin JE, Kozai K, Yoshiko Y (2018) Soluble Klotho causes hypomineralization in Klotho-deficient mice. J Endocrinol 237:285–300

30. The HYP Consortium (1995) A gene (PEX) with homologies to endopeptidases is mutated in patients with X-linked hypophosphatemic rickets. Nat Genet 11:130–136

31. Rowe PS (2004) The wrickkened pathways of FGF23, MEPE and PHEX. Crit Rev Oral Biol Med 15:264–281.

32. David V, Martin AC, Hedge AM, Drezner MK, Rowe PS (2010) ASARM peptides: PHEX-dependent, independent regulation of serum phosphate. Am J Physiol Renal Physiol

300:F783–F791

33. Staines KA, MacRae VE, Farquharson C (2012) The importance of the SIBLING family of proteins on skeletal mineralisation and bone remodelling. J Endocrinol 214:241–255

34. Fisher LW (2001) Flexible structures of SIBLING proteins, bone sialoprotein, and osteopontin. Biochem Biophys Res Commun 280:460–465

35. Butler WT (1995) The nature and functional significance of dentin extracellular matrix proteins Int J Dev Biol 39:169–179

36. Bellahcène A (2008) Small integrin-binding ligand N-linked glycoproteins (SIBLINGs): multifunctional proteins in cancer. Nat Rev Cancer 8:212–226

37. Addison WN, Nakano Y, Loisel T, Crine P, McKee MD (2008) MEPE–ASARM peptides control extracellular matrix mineralization by binding to hydroxyapatite: an inhibition regulated by PHEX cleavage of ASARM. J Bone Miner Res 23:1638–1649

38. Martin A, David V, Laurence JS, Schwarz PM, Lafer EM, Hedge AM, Rowe PS (2008) Degradation of MEPE, DMP1, and release of SIBLING ASARM-peptides (minhibins): ASARM-peptide(s) are directly responsible for defective mineralization in HYP. Endocrinology 149:1757–1772

39. Guo R, Rowe PS, Liu S, Simpson LG, Xiao ZS, Quarles LD (2002) Inhibition of MEPE cleavage by Phex. Biochem Biophys Res Commun 297:38–45

40. Lavi-Moshayoff V, Wasserman G, Meir T, Silver J, Naveh-Many T (2010) PTH increases FGF23 gene expression and mediates the high-FGF23 levels of experimental kidney failure: a bone parathyroid feedback loop. Am J Physiol Renal Physiol 299:F882–F889

41. Luiz de Freitas PH, Li M, Ninomiya T, Nakamura M, Ubaidus S, Oda K, Udagawa N, Maeda T, Takagi R, Amizuka N (2009) Intermittent PTH administration stimulates pre-osteoblastic proliferation without leading to enhanced bone formation in osteoclast-less c-fos(-/-) mice. J Bone Miner Res 24:1586–1597

42. Yamamoto T, Hasegawa T, Sasaki M, Hongo H, Tsuboi K, Shimizu T, Ohta M, Haraguchi M, Takahata T, Oda K, Freitas PHL, Takakura A, Takao-Kawabata R, Isogai Y, Amizuka N (2016) Frequency of teriparatide administration affects the histological pattern of bone formation in young adult male mice. Endocrinology 157:2604–2620

43. Hasegawa T, Endo T, Tsuchiya E, Kudo A, Zhao S, Moritani Y, Abe M, Yamamoto T,

Hongo H, Tsuboi K, Yoshida T, Nagai T, Khadiza N, Yokoyama A, Freitas de PHL, Li M, Amizuka N (2017) Biological application of focus ion beam-scanning electron microscopy (FIB-SEM) to the imaging of cartilaginous fibrils and osteoblastic cytoplasmic processes. J Oral Biosci 59:55–62

44. Hasegawa T, Amizuka N, Yamada T, Liu Z, Miyamoto Y, Yamamoto T, Sasaki M, Hongo H, Suzuki R, Freitas PHL, Yamamoto T, Oda K, Li M (2013) Sclerostin is differently immunolocalized in metaphyseal trabecules and cortical bones of mouse tibiae. Biomed Res 34:153–159

45. Hasegawa T, Yamamoto T, Sakai S, Miyamoto Y, Hongo H, Qiu Z, Abe M, Takeda S, Oda K, Freitas PHL, Li M, Endo K, Amizuka N (2019) Histological effects of the combined administration of eldecalcitol and a parathyroid hormone in the metaphyseal trabeculae of ovariectomized rats. J Histochem Cytochem 67:169–184

46. Hasegawa T, Li M, Hara K, Sasaki M, Tabata C, Freitas PHL, Hongo H, Suzuki R, Kobayashi M, Inoue K, Yamamoto T, Oohata N, Oda K, Akiyama Y, Amizuka N (2011) Morphological assessment of bone mineralization in tibial metaphyses of ascorbic acid-deficient ODS rats. Biomed Res 32:259–269

47. Parfitt AM, Drezner MK, Glorieux FH, Kanis JA, Malluche H, Meunier PJ, Ott SM, Recker RR (1987) Bone histomorphometry: standardization of nomenclature, symbols, and units. Report of the ASBMR Histomorphometry Nomenclature Committee. J Bone Miner Res 2:595–610

48. Biber J, Hernando N, Forster I (2013) Phosphate transporters and their function. Annu Rev Physiol 75:535–550

49. Murali SK, Roschger P, Zeitz U, Klaushofer K, Andrukhova O, Erben RG (2016) FGF23 regulates bone mineralization in a 1,25(OH)2 D3 and Klotho-independent manner. J Bone Miner Res 31:129–142

Figure legends

Figure 1.

Increased trabecular bone and MAR in PTH-administered femora

Panels A and D, B and E, and C and F are obtained from the control femora and femora administered with PTH in the regimen of 2 times/day and 4 times/day, respectively. According to the frequency of PTH administration, the metaphyseal trabeculae seems to be increased (A-C), and thick osteoid can be seen (D-F). Panel G shows the statistical analysis of MAR. Panel H is a graph representing the statistical analysis on the serum Ca and Pi between the control and PTH-administered specimens.

Bars: A–C: 500μm, D–F: 10μm

Figure 2.

Immunolocalization of PHOSPHO1 in the control and PTH-administered femora

Panels A-C and D-F are low and highly magnified images of immunostaining of PHOSPHO1 in the metaphyses of the control (A, D) and PTH-administered (B, C, E, F) femora, respectively. Note that PHOSPHO1-immunoreactivity is mainly seen on the cell surface of mature osteoblasts rather than preosteoblastic cells (arrows in D-F). tb: trabecula

Bars: A–C: 100μm, D–F: 10μm

Figure 3.

Immunolocalization of TNALP and ENPP1 in the control and PTH-administered femora

Panels A-C and D-F are low and highly magnified images of immunostaining of TNALP in the metaphyses of the control (A, D) and PTH-administered (B, C, E, F) femora, respectively. On the other hand, panels G-I and J-L are low and highly magnified images of immunostaining of ENPP1 in the metaphyses of the control (G, J) and PTH-administered (H, I, K, L) femora, respectively. After PTH administration, intense immunoreactivities of TNALP (arrows in E and F) and ENPP1 (arrows in K and L) can be seen. Tb: trabecula

Bars: A–C, G–I: 100μm, D–F, J–L: 30μm

Figure 4.

Immunofluorescent analysis of TNALP and ENPP1 in the control and PTH-administered femora

Panels A-D show immunolocalization of TNALP and ENPP1 in the control specimens, while panels E-H are those obtained from the PTH-administered samples. Panels A and E, B and F, and D and H demonstrate TNALP-, and ENPP1-immunolocalization, and the merged images of TNALP and ENPP1, respectively. Although the uniform distribution of ENPP1 can be seen throughout the control osteoblasts' cytoplasm (arrows in B and D), some osteoblastic cells with intense immunoreactivity of ENPP1 are observed after PTH administration (arrows in F and H). tb: trabecula.

Bars: A–H: 10μm

Figure 5.

Immunolocalization of FGF23, MEPE and osteopontin in the control and PTH administered metaphyseal trabeculae

Panels A-C, D-F and G-I are immunodetection of FGF23, MEPE and osteopontin, respectively. Panels A, D, G show the control metaphyses, while panels B, E, H and C, F, I are from PTH-administered trabeculae with regimens of 2 times or 4 times/day, respectively. FGF23 is observed mainly osteocytes in control specimens (A), while FGF23 can be seen not only in osteocytes but also in osteoblasts after the PTH administration (arrows in B, C). MEPE is observable in osteocytes after the PTH treatment (E, F), while it is hardly detected in the control specimens (D). Note intense osteopontin-immunoreactive cement lines (arrows in H, I) in the PTH-administered specimens, when compared to the control counterpart (G). Tb: trabecula

Bars: A–I: 30μm

Figure 6.

Gene expression of *Tnalp, Enpp1, Phospho1 and Ank* in the control and PTH-administered bones

Panel A reveals RT-PCR assessing gene expression of *Tnalp, Enpp1, Phospho1* and *Ank*, while panels B, C, D and E display the expression of the corresponding genes examined by real time PCR.

Figure 7.

Gene expression of *Mepe, Phex, Fgf23, Fgfr1* and *klotho* assessed by RT-PCR, and of *Mepe, Phex, Fgf23, Fgfr1, Osteopontin, Dmp-1* and *Cathepsin B* by real time PCR

Panel A reveals RT-PCR assessing gene expression of *Mepe, Phex, Fgf23, Fgfr1* and *klotho*, while panels B-H display the gene expression of *Mepe, Phex, Fgf23, Fgfr1, osteopontin, Dmp1* and *Cathepsin B* examined by real time PCR, respectively. Note that only the expression of *Cathepsin B* is significantly reduced after the PTH administration, while the other genes are elevated.

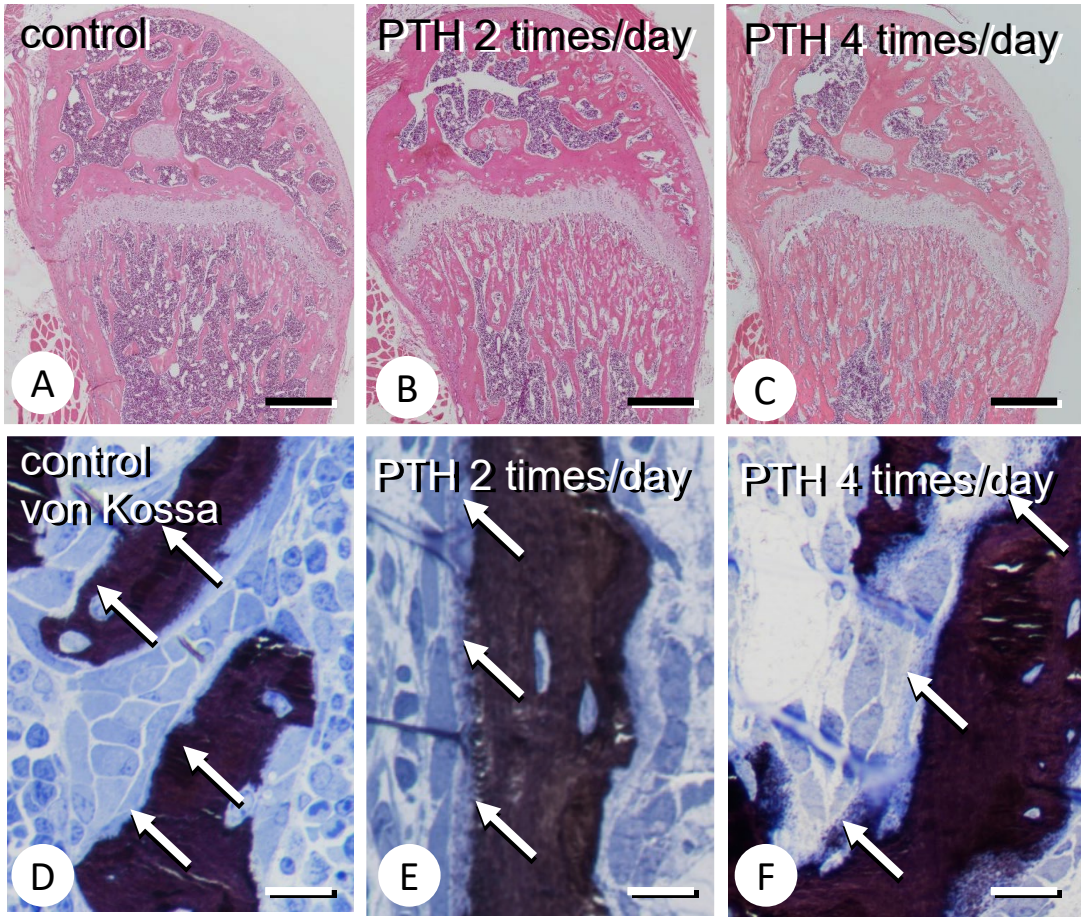
control
PTH 2 times/day
PTH 4 times/day
A
B
C
control
von Kossa
PTH 2 times/day
PTH 4 times/day
D
E
F

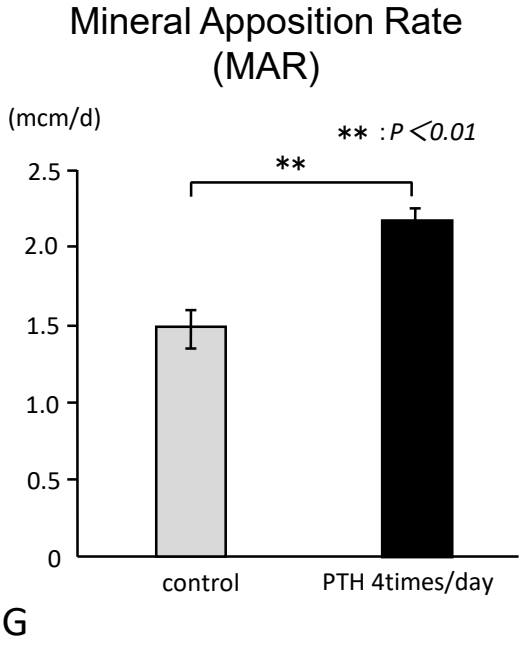
Mineral Apposition Rate
(MAR)
(mcm/d)
** : P < 0.01
**
2.5
2.0
1.5
1.0
0.5
0
control
PTH 4times/day

G

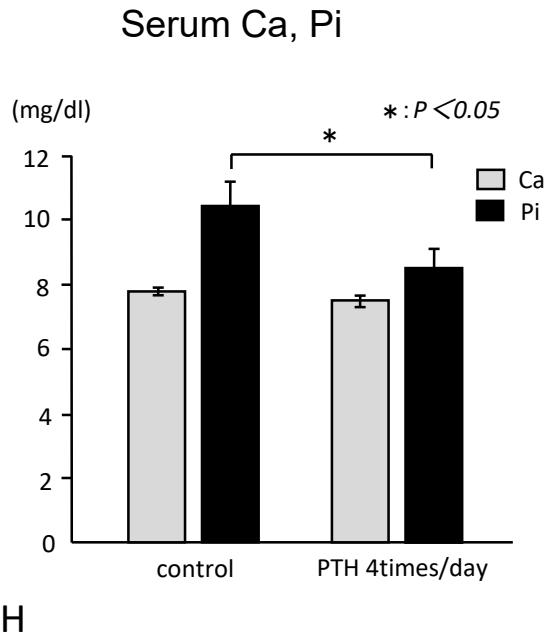
Serum Ca, Pi
(mg/dl)
* : P < 0.05
*
12
10
8
6
4
2
0
Ca
Pi
control
PTH 4times/day

H

Figure 1

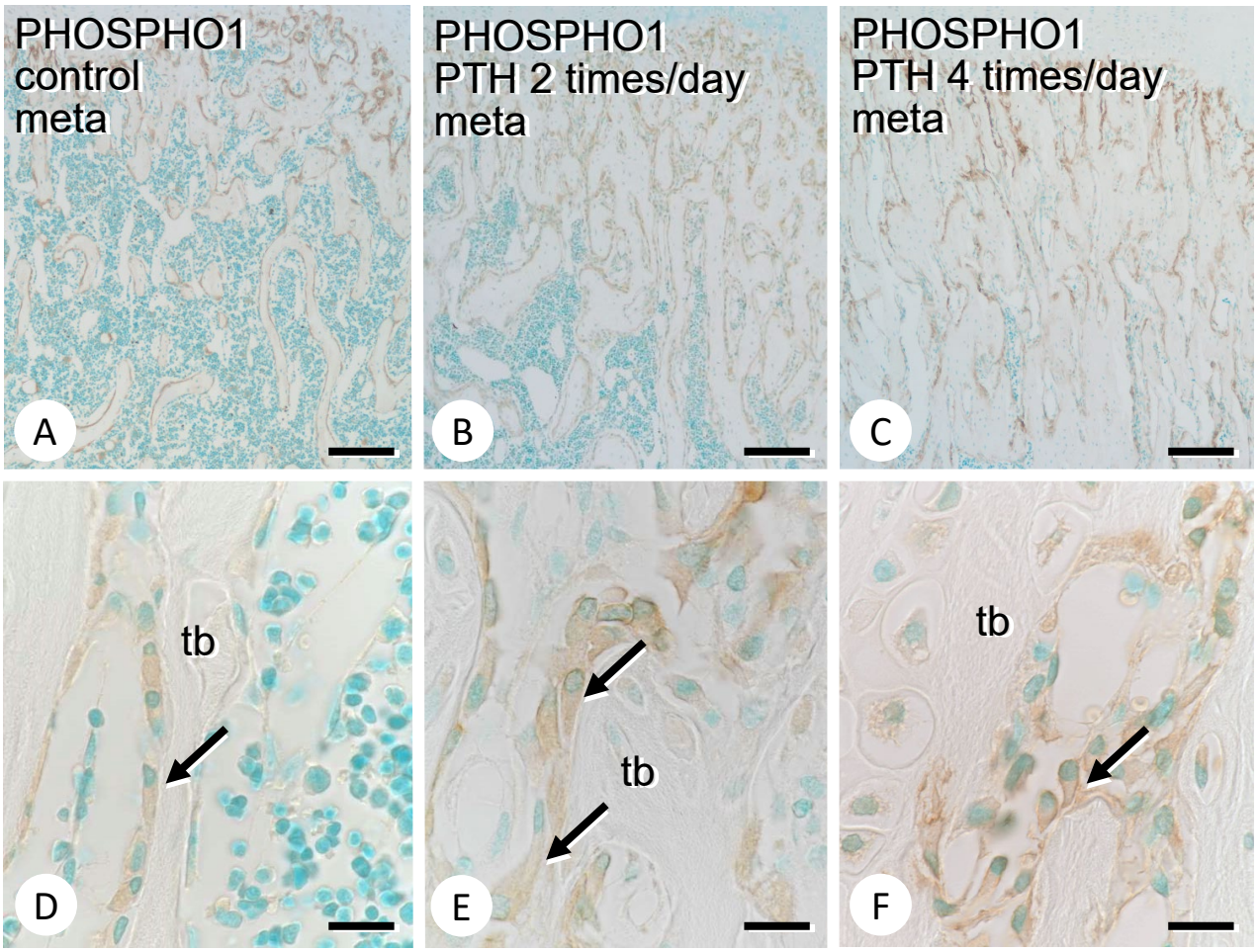
PHOSPHO1
control
meta
A
PHOSPHO1
PTH 2 times/day
meta
B
PHOSPHO1
PTH 4 times/day
meta
C
tb
D
tb
E
tb
F

Figure 2

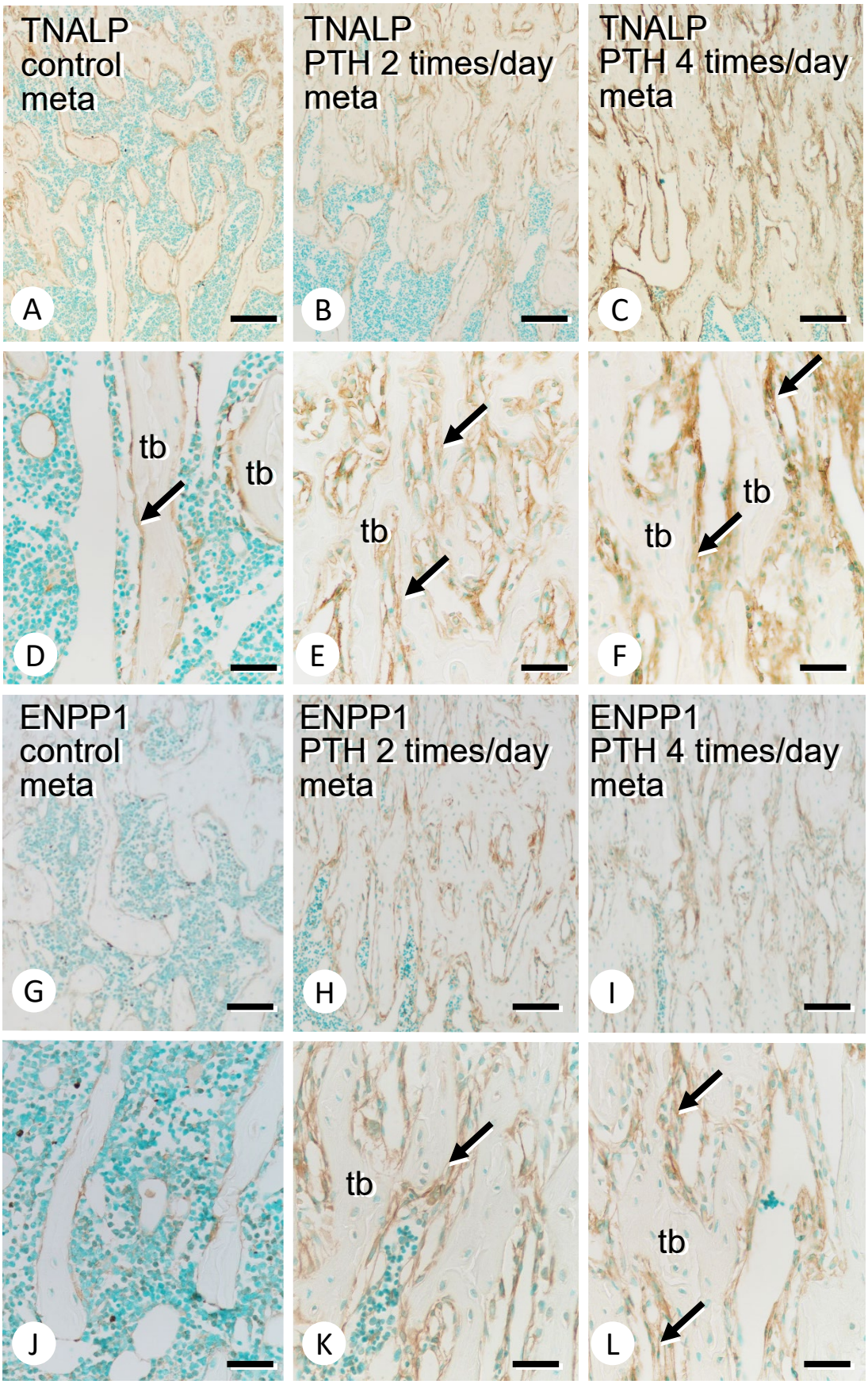
TNALP
control
meta
A
TNALP
PTH 2 times/day
meta
B
TNALP
PTH 4 times/day
meta
C
tb
tb
D
tb
E
tb
tb
F
ENPP1
control
meta
G
ENPP1
PTH 2 times/day
meta
H
ENPP1
PTH 4 times/day
meta
I
J
tb
K
tb
L

Figure 3

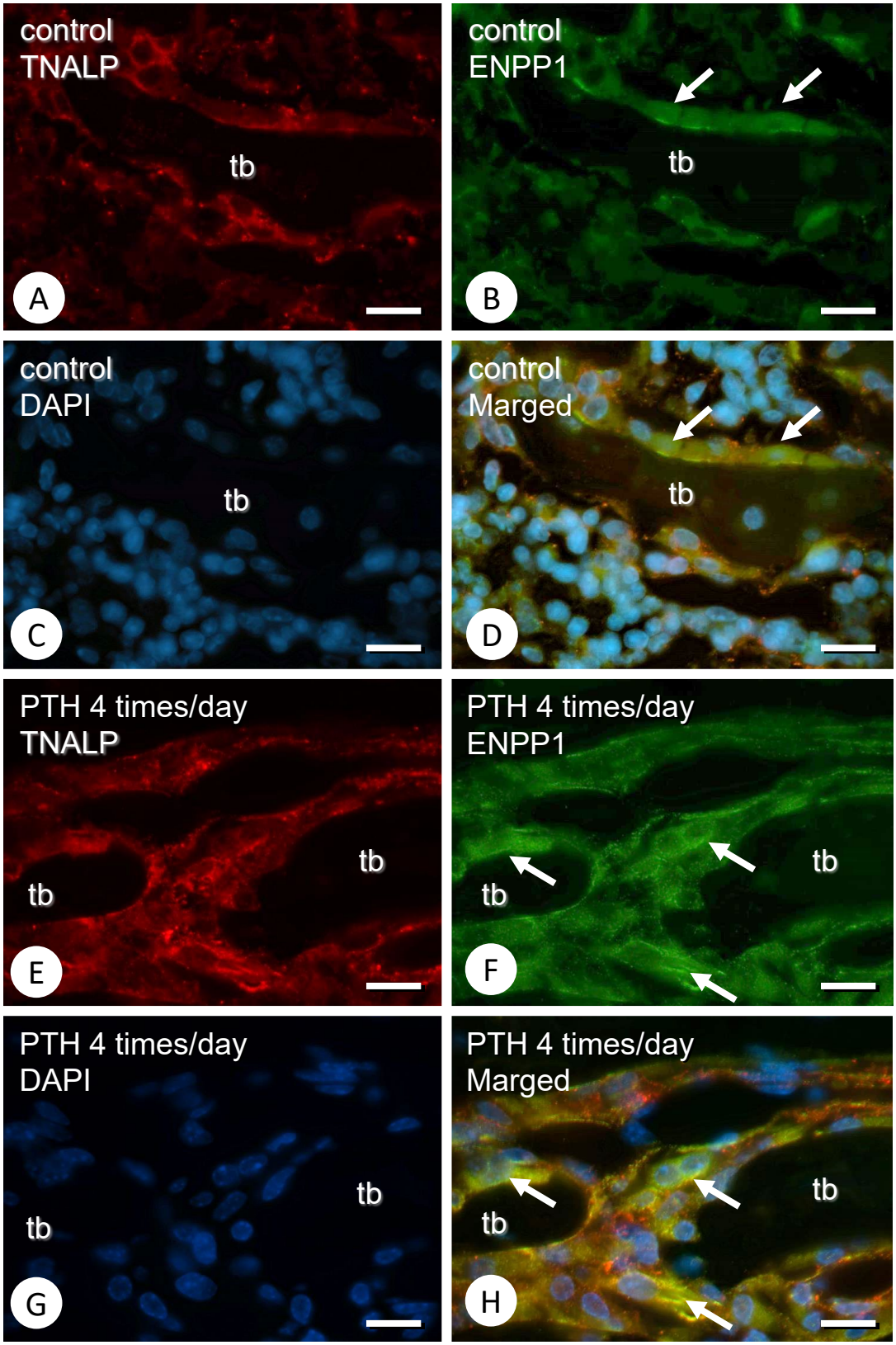
control
TNALP
tb
A
control
ENPP1
tb
B
control
DAPI
tb
C
control
Marged
tb
D
PTH 4 times/day
TNALP
tb
tb
E
PTH 4 times/day
ENPP1
tb
tb
F
PTH 4 times/day
DAPI
tb
tb
G
PTH 4 times/day
Marged
tb
tb
H

Figure 4

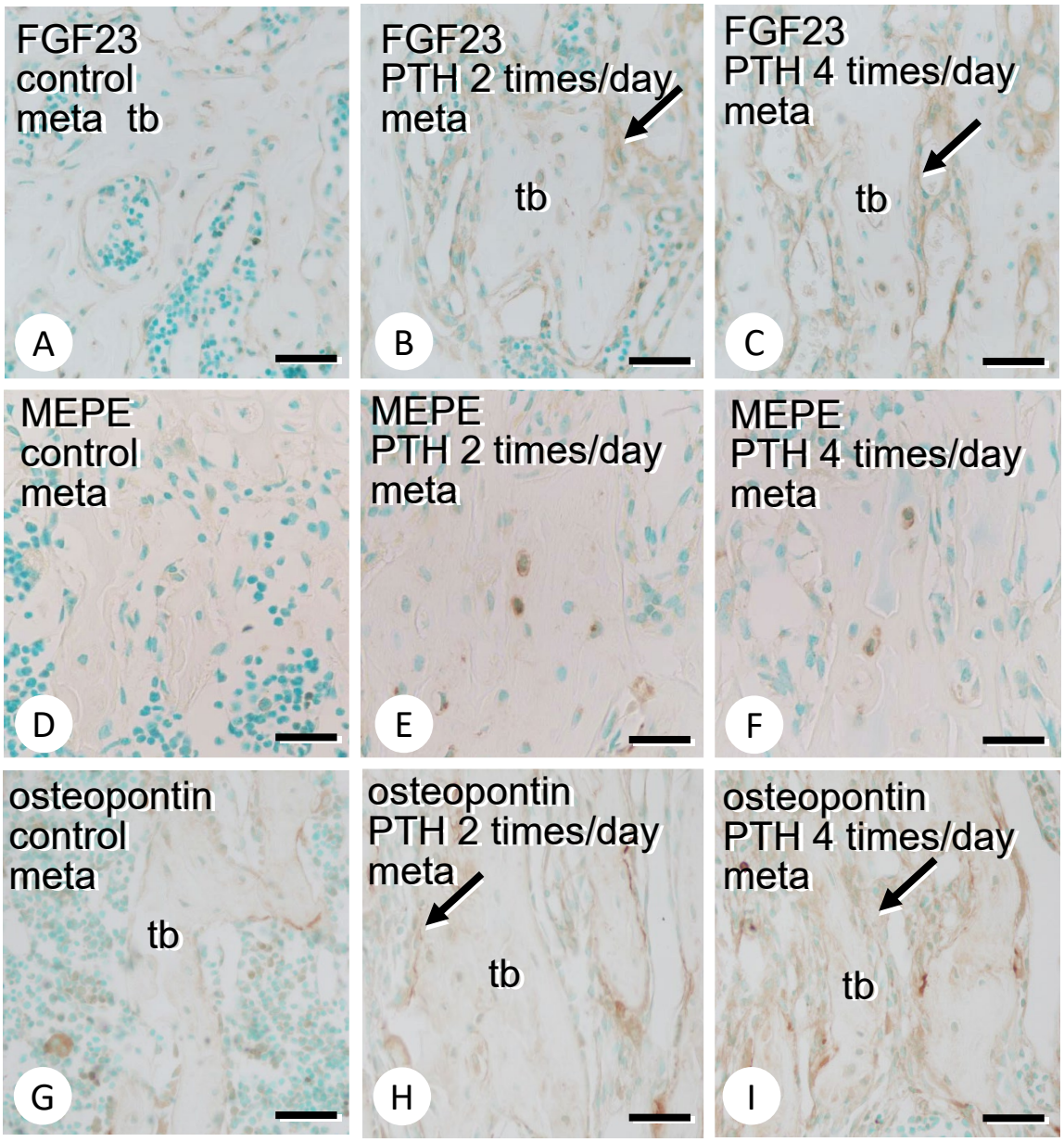
FGF23
control
meta tb
A
FGF23
PTH 2 times/day
meta
tb
B
FGF23
PTH 4 times/day
meta
tb
C
MEPE
control
meta
D
MEPE
PTH 2 times/day
meta
E
MEPE
PTH 4 times/day
meta
F
osteopontin
control
meta
tb
G
osteopontin
PTH 2 times/day
meta
tb
H
osteopontin
PTH 4 times/day
meta
tb
I

Figure 5

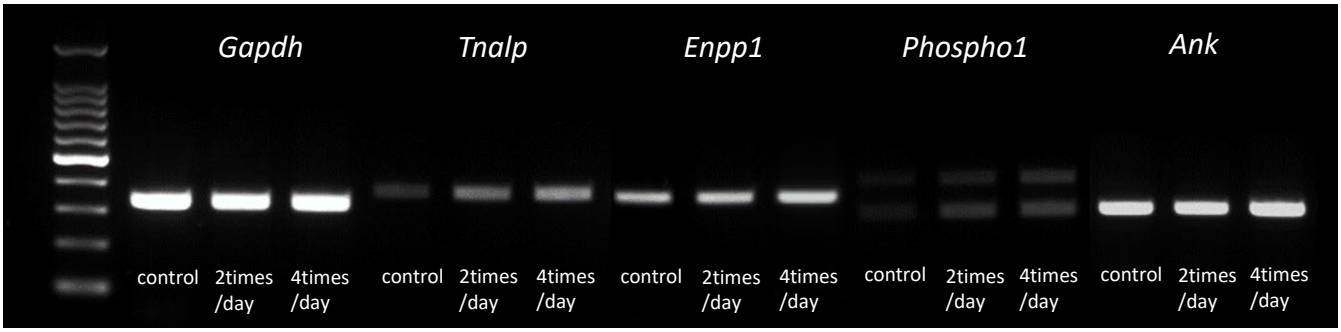

A

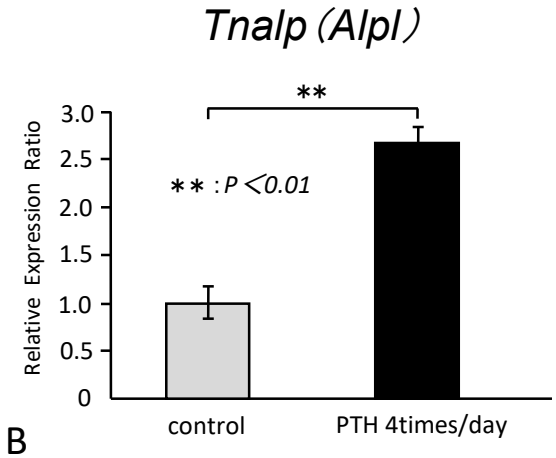

B

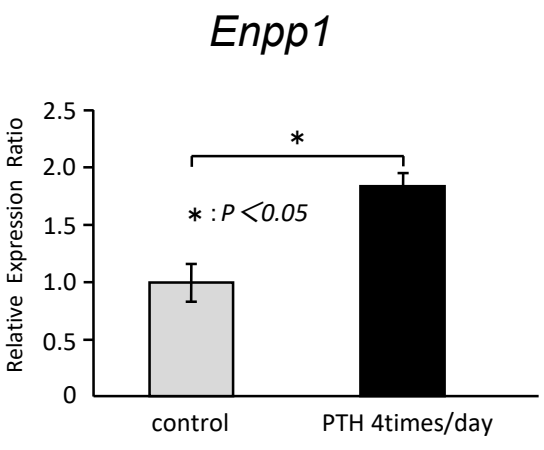

C

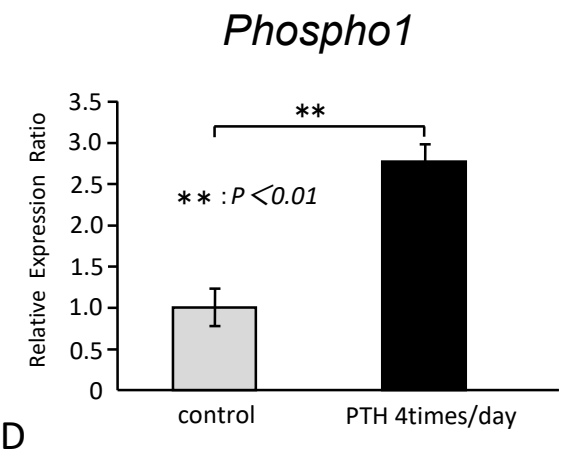

D

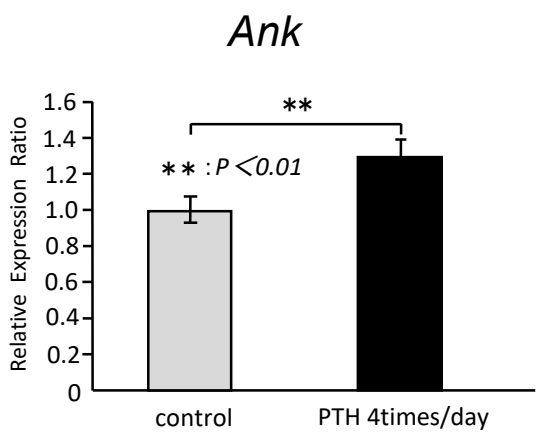

E

Figure 6

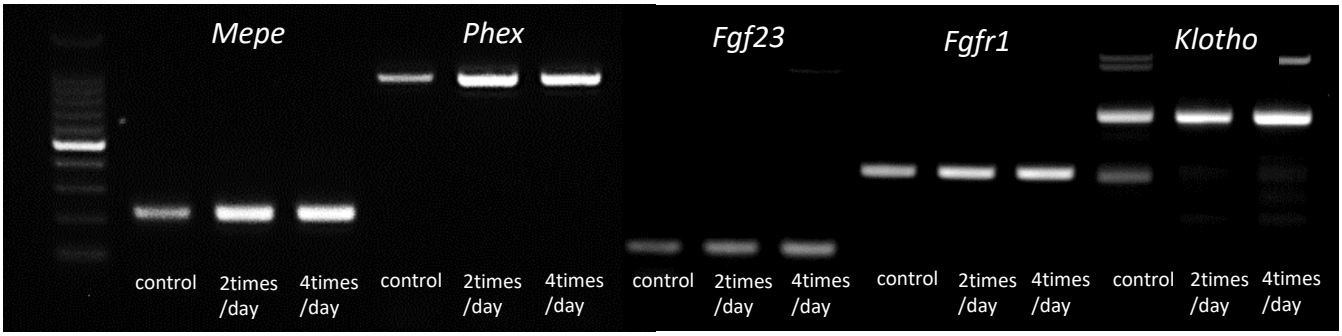

A

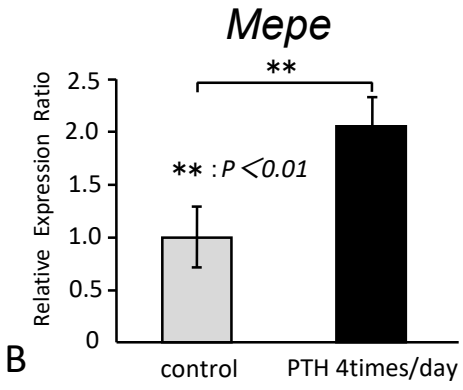

B

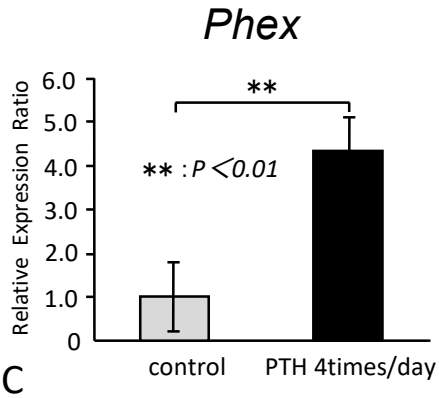

C

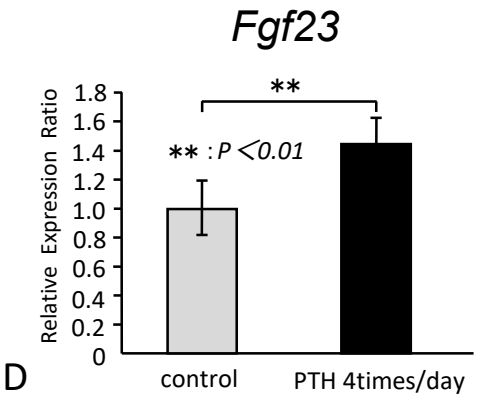

D

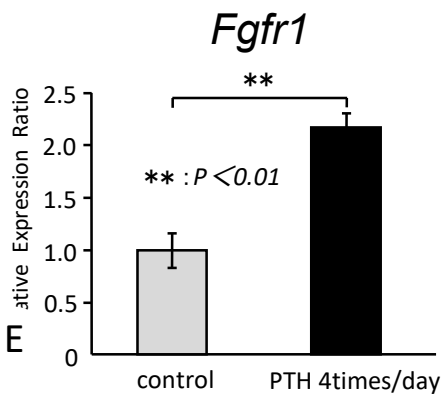

E

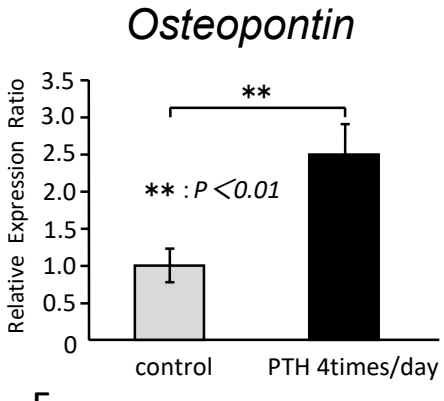

F

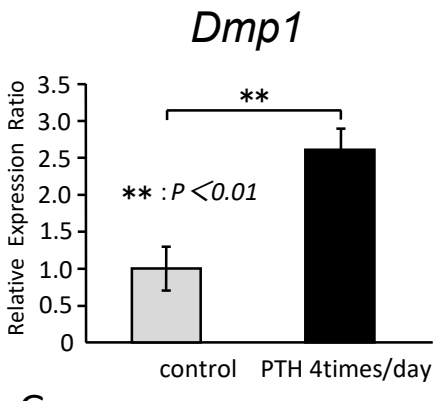

G

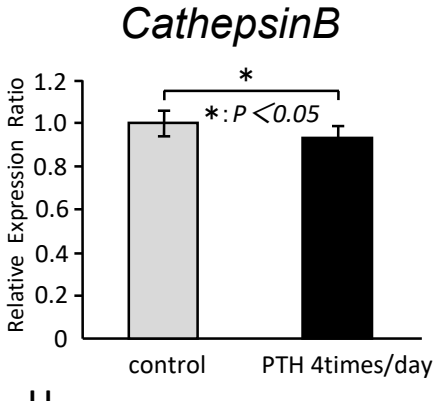

H

Figure 7